Structural basis and mechanism of the unfolding-induced activation of HdeA, a bacterial acid response chaperone

Received for publication, October 23, 2018, and in revised form, December 17, 2018 Published, Papers in Press, December 20, 2018, DOI 10.1074/jbc.RA118.006398

Xing-Chi Yu[‡§1], **Yunfei Hu**[‡§1,2], **Jienv Ding**[§¶3], **Hongwei Li**[‡§], **and Changwen Jin**[‡§¶‖4]

From the [‡]*College of Chemistry and Molecular Engineering,* [§]*Beijing Nuclear Magnetic Resonance Center,* [¶]*College of Life Sciences,* [‖]*Beijing National Laboratory for Molecular Sciences, Peking University, Beijing 100871, China*

Edited by Norma M. Allewell

The role of protein structural disorder in biological functions has gained increasing attention in the past decade. The bacterial acid-resistant chaperone HdeA belongs to a group of "conditionally disordered" proteins, because it is inactive in its well-structured state and becomes activated via an order-to-disorder transition under acid stress. However, the mechanism for unfolding-induced activation remains unclear because of a lack of experimental information on the unfolded state conformation and the chaperone–client interactions. Herein, we used advanced solution NMR methods to characterize the activated-state conformation of HdeA under acidic conditions and identify its client-binding sites. We observed that the structure of activated HdeA becomes largely disordered and exposes two hydrophobic patches essential for client interactions. Furthermore, using the pH-dependent chemical exchange saturation transfer (CEST) NMR method, we identified three acid-sensitive regions that act as structural locks in regulating the exposure of the two client-binding sites during the activation process, revealing a multistep activation mechanism of HdeA's chaperone function at the atomic level. Our results highlight the role of intrinsic protein disorder in chaperone function and the self-inhibitory role of ordered structures under nonstress conditions, offering new insights for improving our understanding of protein structure–function paradigms.

Intrinsically disordered proteins (IDPs)[5] or proteins containing intrinsically disordered regions (IDRs) constitute about a half of human proteins and are often disease-related (1, 2). In prokaryotic proteomes, IDRs are also found to be enriched in proteins involved in pathogenic pathways and essential for invasion of host immune systems (3, 4). Elucidating the functional mechanisms of IDPs or IDRs is critical for understanding the pathogenesis mechanisms of many diseases and is also indispensable for a complete elucidation of the protein structure–function paradigms. However, experimental information of disordered proteins is scarce and remains technically challenging to obtain, mainly due to the intrinsic "fuzziness" of the disordered regions. A group of stress-response chaperones in both eubacteria and eukaryotes have been found to adopt well-folded structures under nonstress conditions and become activated via unfolding under stress conditions (5). These include the redox-regulated Hsp33, the temperature-regulated Hsp26, and the acid-activated chaperone HdeA and are termed "conditionally disordered proteins" (5–10). These proteins represent a unique case of protein disorder, because they undergo an "order-to-disorder" transition during function, which is exactly opposite to the more commonly observed "disorder-to-order" transition either via the "folding-upon-binding" mechanism or by post-translational modifications (11, 12).

The periplasmic chaperone HdeA in enteric bacteria plays a major role during acid stress in protecting a broad range of periplasmic proteins from denaturation-induced aggregation (13–15). The function of HdeA is critical for the survival of pathogenic bacteria when passing through the hosts' stomach, where it interacts with its native clients, including the outer membrane proteins (OMPs) as well as chaperones such as SurA and DegP that are essential in the OMP biogenesis pathways (16, 17). HdeA exists as a well-folded homodimer in the inactive state, and its activation requires acid-induced protein unfolding accompanied by dimer dissociation, resulting in the exposure of hydrophobic surfaces for interaction with denatured client proteins (9–10, 13, 18–23). The molecular mechanism of the unfolding-induced HdeA activation is still unclear, and several long-standing questions remain unanswered concerning the following fundamental aspects. First, what is the active conformation of the HdeA chaperone? Second, where is (are) the client-binding site(s)? Third, how is HdeA activated and what is the structural basis for such an activation, or more specifically, how does acid induce the exposure of the binding site(s)?

This work was supported by Grant 2016YFA0501201 from the National Key R&D Program of China (to C. J.) and Grant 31370718 from the National Natural Science Foundation of China (to Y. H.). The authors declare that they have no conflicts of interest with the contents of this article.

This article contains Figs. S1–S17 and supporting Discussion.

The chemical shift assignments of HdeA-F28W at pH 1.5 have been deposited to the in the BioMagResBank (http://www.bmrb.wisc.edu/) under the accession number of 27693.

[1] Both authors contributed equally to this work.

[2] To whom correspondence may be addressed: Medical College of Soochow University, Suzhou 215123, China. E-mail: yunfei_hu@suda.edu.cn.

[3] Present address: Dept. of Health and Human Services National Institutes of Health, 1050 Boyles St., Frederick, MD 21702.

[4] To whom correspondence may be addressed: Beijing Nuclear Magnetic Resonance Center, College of Life Sciences, College of Chemistry and Molecular Engineering, Peking University, Beijing 100871, China. Tel.: 86-10-62756004; E-mail: changwen@pku.edu.cn.

[5] The abbreviations used are: IDP, intrinsically disordered protein; IDR, intrinsically disordered region; CEST, chemical exchange saturation transfer; FWHM, full width at half-maximum; ITC, isothermal titration calorimetry; PDB, Protein Data Bank; OMP, outer membrane protein; sPRE, solvent paramagnetic relaxation enhancement; HSQC, heteronuclear single quantum coherence; H/D, hydrogen–deuterium; TF, trigger factor.

To address the above issues, we herein employ several state-of-the-art solution NMR techniques that have unique advantages in studying protein disorder and heterogeneous protein–protein interactions at atomic resolution (24–26). The active-state conformation of HdeA has been characterized, which is largely disordered with local residual helical structures. Two hydrophobic segments with relatively extended conformations are identified to play central roles in binding client proteins, and a pH-regulated dynamic equilibrium between the well-folded inactive conformation and a sparsely-populated, partially unfolded conformation is observed. Three pH-sensitive structural regions are identified to function as "structural locks" in regulating the chaperone function activation. Our results provide molecular details of a multistep activation process of HdeA during acid stress, which demonstrates the central role of disordered regions in the chaperone function and the self-inhibitory role of ordered protein structure.

Results

Active-state conformation of HdeA

The inactive HdeA is a homodimer under neutral pH conditions (13, 18, 23), although it becomes unfolded and dissociates into monomers at pH 2 with the estimated K_d value of ~45 μM (13). Under normal sample concentrations for NMR spectroscopy (~100 μM to 1 mM), the activated HdeA is in equilibrium between dimer and monomer conformations, both of which are largely unfolded and show significant signal overlap in the NMR spectra, which greatly hinders spectral analysis (Fig. S1). In this study, we identified a HdeA-F28W mutant that preserves the chaperone activity (Fig. 1, *A* and *B*, and Fig. S2*A*). This mutant is mainly monomeric at low pH judged by size-exclusion chromatography (Fig. S2*B*), and its 2D ^{1}H-^{15}N HSQC spectrum at pH 1.5 shows a unique set of peaks essentially resembling those corresponding to the monomeric conformation of the activated WT-HdeA (Fig. S3). Therefore, the HdeA-F28W mutant can represent the monomeric activated state of HdeA and is used for chemical shift assignments and structural analysis.

By using conventional triple-resonance NMR experiments combined with experiments specifically optimized for disordered proteins, we obtained nearly complete backbone resonance assignments of HdeA-F28W at pH 1.5 (Fig. 1*C*). Analysis of the secondary structural propensity based on chemical shift information (27) confirms that the protein is largely disordered, whereas four short segments show different tendencies of forming local helical conformations (Fig. 1*E*). These residual helical regions generally correspond to part of the original helices α1 to α4 in the inactive HdeA structure, but are significantly shorter in length (Fig. 1, *D* and *E*). The two segments 20–24 and 61–67 that are linked to each other via the strictly conserved disulfide bond between cysteine residues 18 and 66 show close to 40 and 70% helical contents, whereas the other two segments 35–43 and 79–83 display lower helix-forming tendencies. The results are in accordance with the relaxation parameter R_2/R_1 ratios, with higher R_2/R_1 ratios indicating less structural flexibility. The averaged R_2/R_1 value for segments 20–24 and 61–67 is ~13.6, which is approximately two times the value of ~7.4 for segments 35–43 and 79–83, and it is significantly higher than the N terminus of the sequence (Fig. 1*E*). This indicates that residual structures are present in the above regions, and the local conformation around the disulfide bond maintains the highest rigidity.

Site-specific ^{19}F labeling in HdeA

As demonstrated in our previous study (23), the majority of the backbone amide signals of HdeA in the ^{1}H-^{15}N HSQC spectra disappear upon binding to client proteins, and the remaining observable resonances correspond to the flexible, charged N and C termini (Fig. 1*A*). All signals throughout the 14–72 region are unobservable, making it impossible to identify residues that are most critical for client interactions. We therefore used ^{19}F NMR spectroscopy to characterize the conformational properties of activated HdeA in both the client-free and -bound states by site-specifically introducing ^{19}F-labeled tryptophan into the protein sequence. Considering that the tryptophan residue contains a bulky hydrophobic side chain, which could potentially disrupt protein structure as well as affect chaperone–client interactions, the conformational states and chaperone-like activities of all mutants were carefully examined and compared with WT-HdeA. A total of 15 mutants containing site-specifically incorporated ^{19}F-labeled tryptophan (Fig. 2*A*) was selected and used for further ^{19}F NMR experiments, and the naming follows a "HdeA-*xx*-fluoro" pattern, where "*xx*" is the number for the amino acid position with the ^{19}F label in the protein primary sequence (Table 1). ^{1}H-^{15}N HSQC spectra were recorded to confirm that the mutations do not disrupt the overall structure of the inactive state and also do not interfere with client binding (Fig. S4). Isothermal titration calorimetry (ITC) experiments (Fig. S5) and anti-aggregation assays (Fig. S6) further verified that the mutant retains chaperone activities essentially similar to WT-HdeA. One-dimensional ^{19}F NMR spectra were collected at pH 7.0 and 2.0 for all ^{19}F-labeling sites (Fig. S7 and S8), and the results show that the ^{19}F chemical shifts are dispersed over a range of ~5 ppm (−47.7 to −52.5 ppm) at pH 7 while clustering around −48.3 ppm at pH 2, which is consistent with acid-induced unfolding (see more details in supporting Discussion).

It is worth mentioning that among the 15 sites for ^{19}F incorporation, 10 sites showed a unique peak in the ^{19}F NMR spectra of the free state at pH 2.0, whereas mutations to tryptophan in the remaining five sites (residue numbers 16, 24, 35, 78, and 82) resulted in the detection of two or more resonance peaks (Fig. S8). In particular, the HdeA-24-fluoro, HdeA-35-fluoro, HdeA-78-fluoro, and HdeA-82-fluoro mutants show two peaks at pH 2, originating from a dynamic equilibrium between dimer and monomer conformations as indicated by concentration-dependent changes of peak intensities in both ^{19}F NMR and ^{1}H-^{15}N HSQC spectra. In addition, the HdeA-16-fluoro mutant appears to be structurally more stable at acidic pH compared with WT-HdeA, as it still harbors the folded conformation at pH 2.0 as shown by the ^{1}H-^{15}N HSQC spectra (Fig. S8*A*). This sample shows a total of four peaks in the ^{19}F NMR spectrum at acidic pH, as similarly observed in a previous study that identified the two peaks on the left as originating from the folded (or locally folded) conformation (28). Concentration-dependent ^{19}F NMR data further identified the monomeric and dimeric states of the

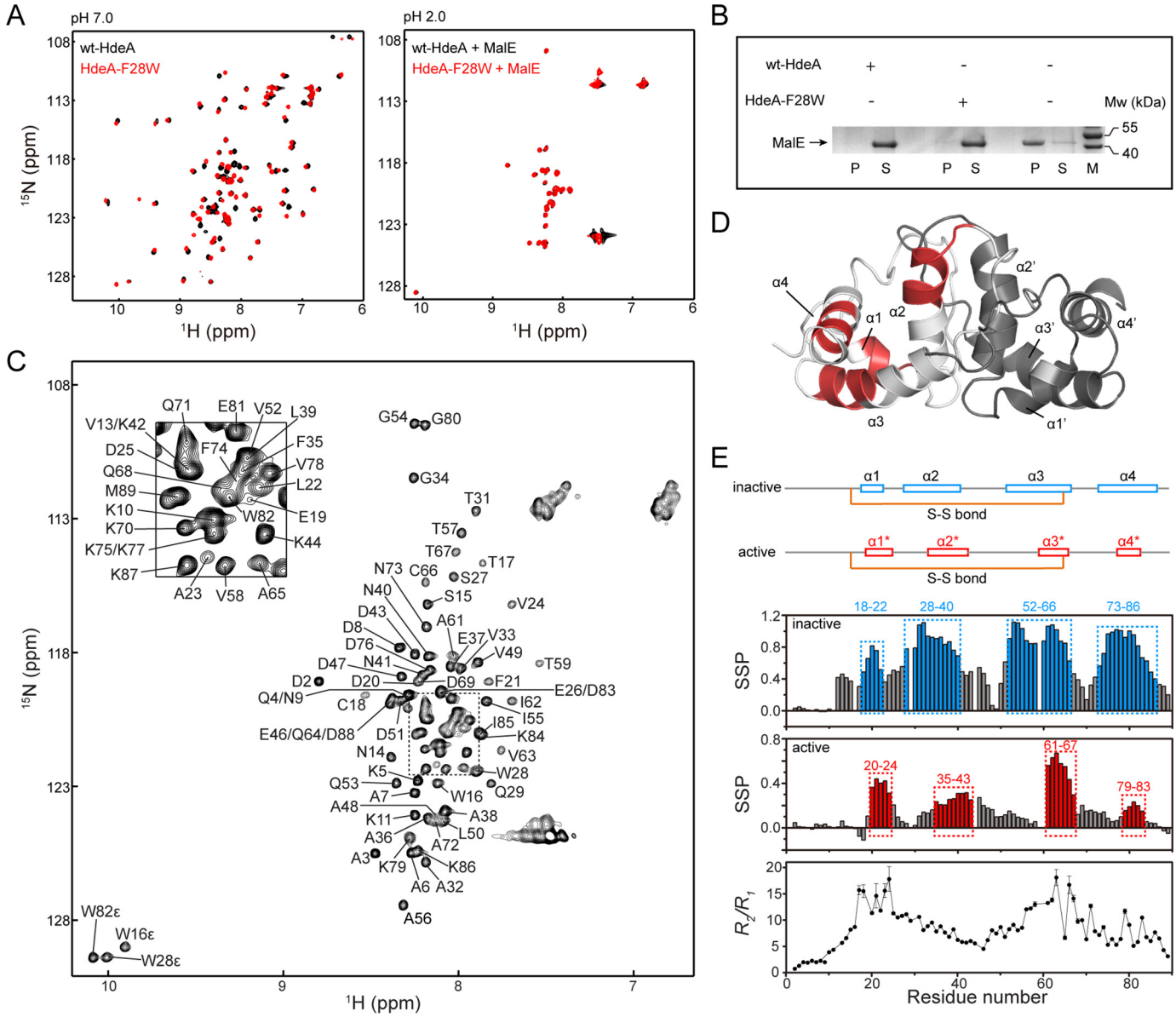

Figure 1. Structural characterization of HdeA in the activated state. *A,* overlay of the ^{1}H-^{15}N HSQC spectra of ^{15}N-labeled WT-HdeA (*black*) and HdeA-F28W mutant (*red*) at pH 7.0 (*left panel*) or in the presence of excess unlabeled MalE at pH 2.0 (*right panel*). *B,* chaperone activities of WT-HdeA and HdeA-F28W mutant were assayed by incubating the client protein MalE under acidic conditions in the presence or absence of the chaperone and semi-quantitatively follow the appearance of the MalE in either the supernatant or the precipitant as described previously (9, 43). The sample of MalE (10 μM) was incubated at pH 1.5 in the presence of equimolar WT-HdeA (*left panel*), HdeA-F28W (*middle panel*), or alone (*right panel*) for 60 min. *P*, *S*, and *M* represent the precipitant, the supernatant, and protein marker, respectively. *C,* ^{1}H-^{15}N HSQC spectrum of HdeA-F28W mutant at pH 1.5 annotated with the backbone resonance assignments. *D,* mapping of the residual helical regions (colored *red*) onto the folded HdeA dimer structure (PDB entry 5WYO). The two molecules in the HdeA dimer are shown in *gray* and *black*, with the α-helices labeled as *α1–α4* and *α1′–α4′*, respectively. *E,* structural analyses of HdeA-F28W at pH 1.5 showing the secondary structural propensity (*SSP*) scores (*middle panel*) and the ratios of the backbone ^{15}N relaxation transverse and longitudinal rates R_2/R_1 (*lower panel*), with regions showing the propensities of forming secondary structures shown in *red* in the *middle panel*. The SSP scores were calculated based on the chemical shifts of $^{13}C^{\alpha}$ and $^{13}C^{\beta}$ atoms using the program package SSP (27). SSP scores close to 1 indicate high propensity of α-helices. The R_1 and R_2 relaxation rates were measured on a 700-MHz spectrometer. For comparison, the SSP scores of the inactive HdeA based on the chemical shift assignments of WT-HdeA at pH 3.0 (23) is also shown (*upper panel*, helical regions shown in *blue*). The helical elements α1–α4 in the inactive state (*blue*) and α1*–α4* in the active state (*red*) are schematically shown on the *top*. The intramolecular disulfide bond is formed between cysteine residues 18 and 66.

unfolded conformation (Fig. S8*B*). For these mutants, chemical shift and line-shape analyses of the ^{19}F NMR data were performed using the peak corresponding to the monomeric unfolded conformation.

Client-binding sites identified by ^{19}F NMR

To identify the regions responsible for binding client proteins, we measured the solvent isotope shifts $\Delta\delta = \delta(D_2O) - \delta(H_2O)$ (26) for each labeling site at pH 2.0 in the absence or presence of a native client protein MalE (Fig. 2*B* and Fig. S9) 16). All $\Delta\delta$ values are negative, and those closer to zero (smaller $|\Delta\delta|$ values) indicate less solvent exposure. Therefore, we expect that the regions of HdeA in direct contact with the client protein to be buried show the smallest $|\Delta\delta|$ values in the complex sample. In addition, we also expect to see a decrease of solvent exposure (thus negative $\Delta\Delta\delta$ values, when $\Delta\Delta\delta$ is calculated as

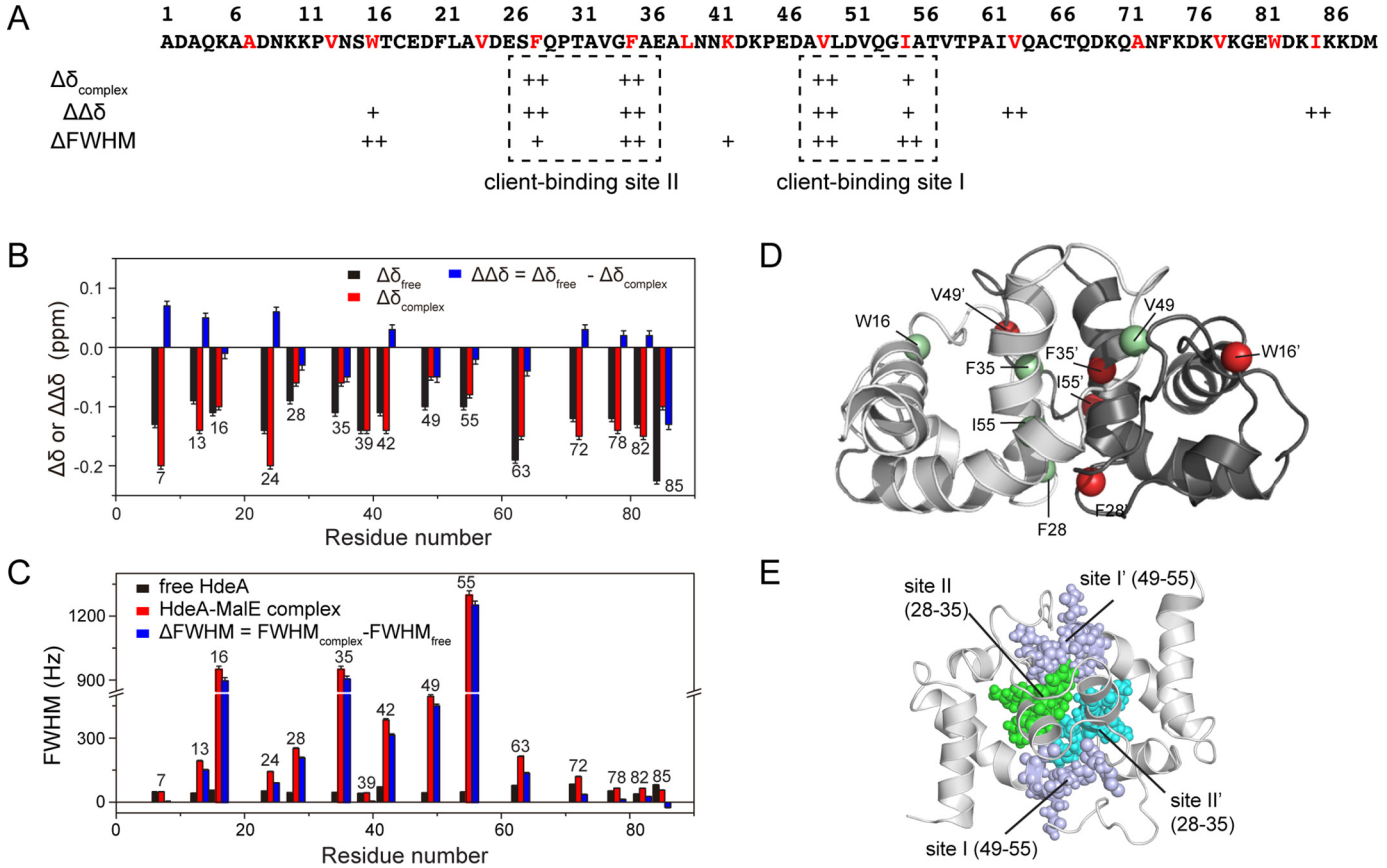

Figure 2. HdeA–client interactions probed by ^{19}F NMR. *A,* amino acid sequence of WT-HdeA showing the positions for site-specific incorporation of ^{19}F probe (colored *red*) and the two client-binding sites. *B,* solvent-induced isotope shifts $\Delta\delta$ of site-specifically ^{19}F-labeled HdeA mutants in the free and complexed state at pH 2.0, and the difference $\Delta\Delta\delta$ between the two. The $\Delta\delta$ values are calculated as $\Delta\delta = \delta(D_2O) - \delta(H_2O)$, where $\delta(D_2O)$ is the ^{19}F chemical shift measured in 100% D_2O, and $\delta(H_2O)$ is that measured in 90% H_2O and 10% D_2O. All $\Delta\delta_{free}$ and $\Delta\delta_{complex}$ values are negative, and those closer to zero indicate less solvent exposure in the complexed state and higher possibility of involvement in client binding. The $\Delta\Delta\delta$ values are calculated as $\Delta\Delta\delta = \Delta\delta_{free} - \Delta\delta_{complex}$, with negative $\Delta\Delta\delta$ values indicating less solvent exposure upon client binding. The more negative $\Delta\Delta\delta$ value indicates a larger decrease of solvent exposure upon client binding and thus a higher possibility of involvement in client binding. *C,* full-width at half-maximum (FWHM) values of site-specifically ^{19}F-labeled HdeA mutants in the free and complexed state at pH 2.0 and the difference ΔFWHM between the two. The ΔFWHM values are calculated as $\Delta\text{FWHM} = \text{FWHM}_{complex} - \text{FWHM}_{free}$, with larger ΔFWHM values indicating client binding. The values $\Delta\delta_{complex}$, $\Delta\Delta\delta$, and ΔFWHM were independently used as criteria to judge whether the ^{19}F-labeled sites are involved in client binding, and the results are indicated *below* the protein sequence in *A*. ^{19}F-Labeled sites with $\Delta\delta_{complex}$ values satisfying 0 ppm $\leq \Delta\delta_{complex} \leq -0.07$ ppm, $\Delta\Delta\delta$ values satisfying $\Delta\Delta\delta \leq -0.025$ ppm, or ΔFWHM values satisfying $\Delta\text{FWHM} \geq 400$ Hz are marked by "++" in *A*; those with $\Delta\delta_{complex}$ values satisfying -0.07 ppm $< \Delta\delta_{complex} \leq -0.10$ ppm, $\Delta\Delta\delta$ values satisfying -0.025 ppm $< \Delta\Delta\delta < 0$ ppm, or ΔFWHM values satisfying 200 Hz $\leq \Delta\text{FWHM} <$ 400 Hz are marked by "+" in *A* (see supporting Discussion for more details). *D,* mapping of the ^{19}F-labeled sites that show direct involvement in client binding onto the HdeA dimer structure. Residues from the two monomers are shown as *green* and *red spheres*, respectively. *E, ribbon* diagram of HdeA dimer structure with the client-binding sites from both molecules shown as *spheres*. Site I from both monomers are colored in *light blue*, and site II from the two molecules are colored in *green* and *cyan*.

$\Delta\delta_{free} - \Delta\delta_{complex}$ as shown in Fig. 2*B*) for residues involved in interaction when comparing the complexed state with the free state. Both criteria unambiguously support the identification of two hydrophobic regions 28–35 and 49–55 as the interaction sites. Residue Trp-16 also appears to contribute to client binding, suggested by the decreased $|\Delta\delta|$ value in the complex state compared with the free state. However, this position exhibits limited solvent exposure in the free state as well, possibly due to the residual secondary structures around the disulfide bond region.

Furthermore, comparison of the signal line widths in the free and complexed states at pH 2.0 supports the participation of segments 28–35, 49–55, as well as residue 16 in binding client proteins (Fig. 2*C*). The significantly increased line widths of these residues in the presence of the client protein demonstrate direct involvement in binding, whereas the nearly unchanged chemical shifts for all positions reflect the heterogeneous (or promiscuous) nature of the binding. Particularly, site 55 shows significant line broadening and apparently comprises multiple conformations, indicative of heterogeneous binding (Fig. 3).

Taking all the above factors into consideration, it is clear that the two segments that are rich in hydrophobic residues, namely the 28–35 and 49–55 segments, play central roles in directly binding to unfolded client proteins under acid stress (Fig. 2*A*). The ^{19}F-labeling sites identified to participate in client interactions are mapped onto the folded HdeA dimer structure in Fig. 2*D*, whereas space-filling representation of the two segments showing their locations in the dimer structure are depicted in Fig. 2*E*. Taking into account that the 28–35 segment is more deeply buried in the core of the dimer, we herein term the 49–55 segment as client-binding site I and the 28–35 segment as client-binding site II (see below).

To further verify these two client-binding sites, four single mutants HdeA-F28K, HdeA-V33K, HdeA-V49K, and HdeA-

Table 1
Summary of HdeA mutants used in this study

Nomenclature	Description	
wt-HdeA	wild-type HdeA	
HdeA-F28W	a single mutation with residue Phe28 substituted by tryptophan; mimics the monomeric active state at pH 1.5	
HdeA-NΔ9	residues A1-N9 deleted	
HdeA-F28K	a single mutation with residue Phe28 substituted by lysine	
HdeA-V33K	a single mutation with residue Val33 substituted by lysine	
HdeA-V49K	a single mutation with residue Val49 substituted by lysine	
HdeA-L50K	a single mutation with residue Leu50 substituted by lysine	
Mutants for site-specific ^{19}F-labeling		
^{19}F-labeling site	**Nomenclature**	**Mutations**
7	HdeA-7-fluoro	A7W/W16F/W82F
13	HdeA-13-fluoro	V13W/W16F/W82F
16	HdeA-16-fluoro	W82F
24	HdeA-24-fluoro	V24W/W16F/W82F
28	HdeA-28-fluoro	F28W/W16F/W82F
35	HdeA-35-fluoro	F35W/W16F/W82F
39	HdeA-39-fluoro	L39W/W16F/W82F
42	HdeA-42-fluoro	K42W/W16F/W82F
49	HdeA-49-fluoro	V49W/W16F/W82F
55	HdeA-55-fluoro	I55W/W16F/W82F
63	HdeA-63-fluoro	V63W/W16F/W82F
72	HdeA-72-fluoro	A72W/W16F/W82F
78	HdeA-78-fluoro	V78W/W16F/W82F
82	HdeA-82-fluoro	W16F
85	HdeA-85-fluoro	I85W/W16F/W82F

L50K were constructed and were observed to show decreased chaperone activity compared with WT-HdeA (Fig. S10, *A* and *B* and supporting Discussion). Notably, single mutation of either Val-33 in client-binding site II or Leu-50 in site I to lysine disrupts the folding of HdeA in its inactive form at pH 7, whereas the F28K and V49K mutants maintains the well-folded dimeric structure at neutral pH (Fig. S10*C*). These observations can be attributed to the facts that the side chains of Val-33 and Leu-50 largely contribute to packing of the hydrophobic core, whereas those of Phe-28 and Val-49 point toward the periphery of the dimer structure. Nevertheless, all four mutants are largely disordered at pH 1.5, which is similar to WT-HdeA. The four mutations do not prevent the acid-induced unfolding of HdeA, and the V33K and L50K mutations even result in constitutive unfolding at neutral pH. The deficiency of these mutants in preventing acid-induced client precipitation supports the role of these two sites in client binding.

Furthermore, it is worth noting that both client-binding sites are sandwiched between regions with relatively high propensities of residual helical conformations but display low propensities themselves (<20%) of forming helices in the active state (Fig. 1*E*). Site II contributes to the formation of a large portion of the helix α2 in the inactive dimer structure, whereas the ^{52}VQGI^{55} tetra-peptide in site I forms the N-terminal tip of helix α3. The transition from helical to the more extended random coil conformation may be important for exposure of the hydrophobic residues and thus interaction with client proteins.

pH-regulated order-to-disorder transition

The order-to-disorder transition of HdeA during acid stress that exposes the two client-binding sites can be probed by the pH-dependent solvent paramagnetic relaxation enhancement (sPRE) experiment, which uses soluble paramagnetic probes to characterize the solvent accessibility of each residue. The results show that the inactive HdeA dimer structure is relatively compact at pH 6, with the majority of the residues minimally affected by the paramagnetic probes, whereas several regions, including the N and C termini as well as the two client-binding sites, show significantly increased solvent accessibility at pH 4 and 3 (Fig. 4) and is in general agreement with the NMR hydrogen/deuterium (H/D) exchange data previously reported (22).

To provide direct experimental characterizations of the partially unfolded intermediates along the pH-dependent unfolding pathway of HdeA, we further used the chemical exchange saturation transfer (CEST) NMR method that has special advantages in probing sparsely-populated protein conformations (25, 29). Briefly, when the structure of a protein is in exchange between a highly-populated ground state and a sparsely-populated "invisible" (or "excited") state, saturation on the sparsely-populated state could be transferred to the ground state and result in the signal intensity reduction of the ground state, thus rendering the invisible state to become "visible." ^{15}N-CEST NMR spectra of the WT-HdeA were systematically recorded at pH values of 4.0, 3.5, 3.0, and 2.5 (Fig. S11). The HSQC spectra in the pH range of 4.0–3.0 show a single set of peaks corresponding to the folded dimeric state, and therefore the ^{15}N-CEST profiles are probing conformational exchanges with the folded dimer as the ground state. However, the HSQC spectrum of WT-HdeA at pH 2.5 is highly heterogeneous and contains multiple sets of peaks, including one set corresponding to the folded dimer similar to that detected at pH 3.0, as well as those similar to the unfolded states (which is an equilibrium of unfolded dimer and monomer states) as detected at pH 2.0 (Fig. S12). Only the CEST profiles of resonances corresponding to the dimer species were analyzed, and thus the ^{15}N-CEST data at pH 2.5 presented herein also report on the conformational exchanges with the folded dimer as the ground state. The experiments detected no excited states for all residues at pH 4.0, whereas sparsely-populated excited conformations were observed for a certain number of residues in the pH range of 3.5 to 2.5, many of which show chemical shifts resembling random coils (Fig. 5, *A* and *B*, and Fig. S11) (30). The number of residues harboring the excited state increases as the pH decreases, and a drastic difference was observed between pH conditions of 3.0 and 2.5 (Fig. 5*A*). At pH 2.5, when HdeA is highly activated, over half of the total number of residues show exchanges between folded and unfolded conformations, and the residues are spread out in the protein sequence, suggesting that the exchange process corresponds to a global unfolding of

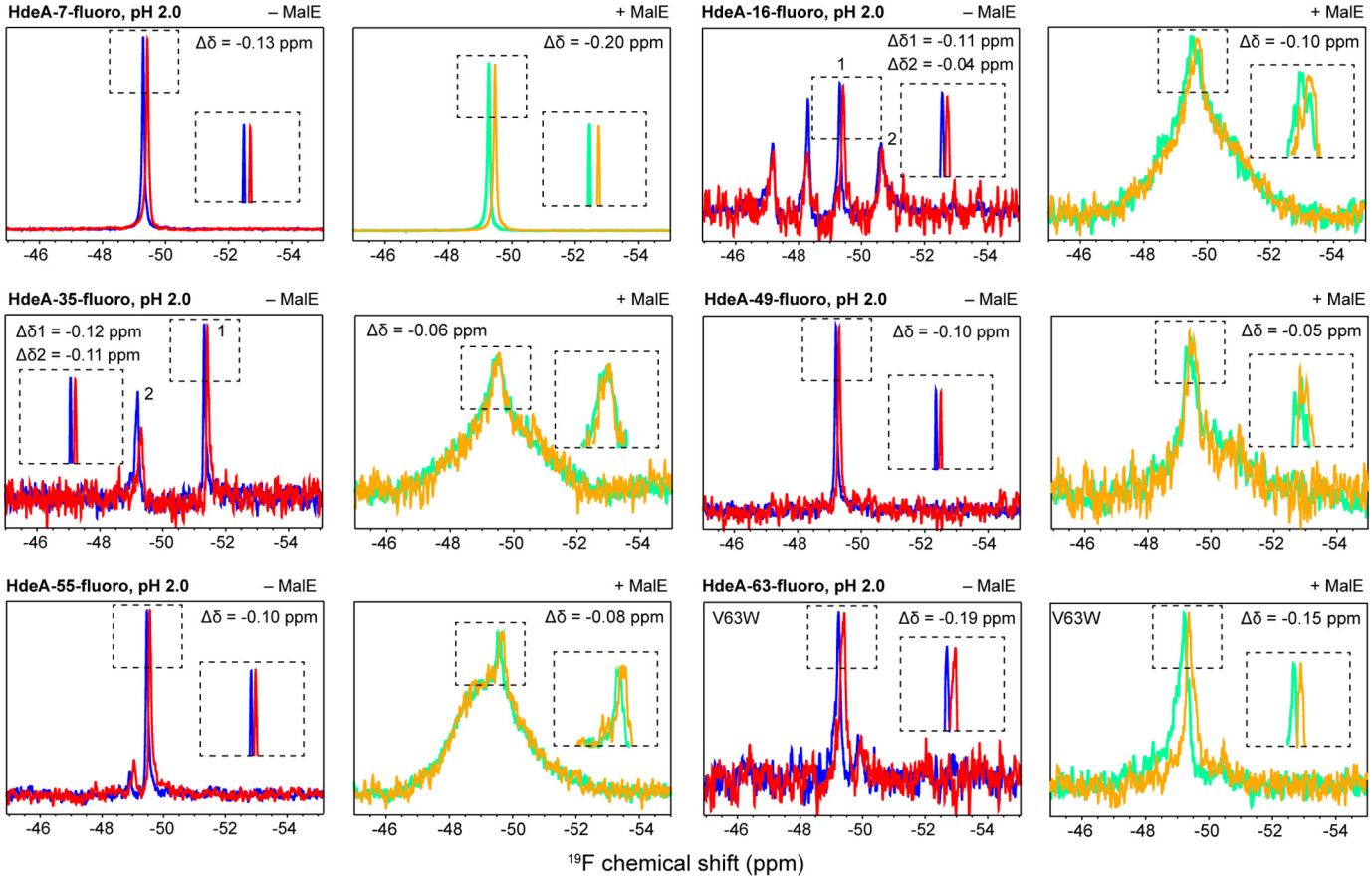

Figure 3. Representative ^{19}F NMR spectra of HdeA. Representative ^{19}F NMR spectra of HdeA mutants with ^{19}F probes incorporated at sites 7, 16, 35, 49, 55, and 63 in the free state (*left*) or in complex with the client protein MalE (*right*) at pH 2.0. The spectra acquired in a buffer containing 90% H_2O and 10% D_2O are shown in *blue* or *green* for the free or complexed state, and those acquired in 100% D_2O are shown in *red* or *yellow* for the free or complexed state. Enlarged view of the peaks are shown as *insets*.

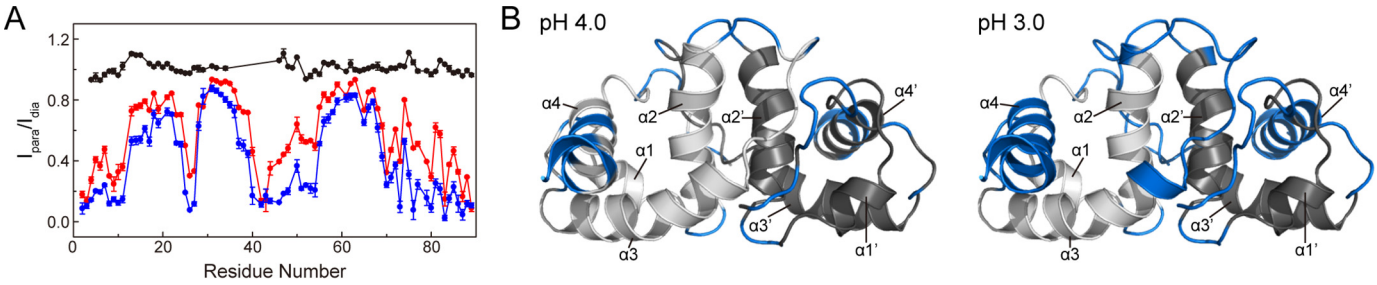

Figure 4. sPRE profiles of WT-HdeA at different pH values. *A,* sPRE effect for each residue was presented by the intensity ratio of the paramagnetic and diamagnetic samples (I_{para}/I_{dia}). Higher solvent accessibility results in a lower I_{para}/I_{dia} ratio. The data obtained at pH 6.0, 4.0, and 3.0 are shown in *black, red,* and *blue*, respectively. *B,* residues that show I_{para}/I_{dia} ratio lower than 0.4 are colored blue in the HdeA dimer structure at pH 4.0 (*left panel*) and 3.0 (*right panel*).

the protein structure. This is further supported by the high correlation between the excited state chemical shifts of WT-HdeA at pH 2.5 with the active disordered state chemical shifts obtained from the assignments of HdeA-F28W at pH 1.5 (Fig. S13). Notably, the HSQC spectrum of WT-HdeA at pH 2.5 contains signals originating from the unfolded conformation, and thus the minor peaks detected in the CEST profiles should be detectable in the HSQC spectrum, although accurate identifications of these peaks are difficult due to the severe signal overlaps originating from dimer–monomer equilibrium of unfolded WT-HdeA. In contrast, order-to-disorder conformational exchanges occur only at local regions at pH 3.0 and above, and these partially unfolded conformations most probably represent the unfolding intermediates along the pH-induced activation pathway.

Global fitting analyses of the CEST data using a two-state exchange model, $G \underset{k_{EG}}{\overset{k_{GE}}{\rightleftharpoons}} E$, where G and E stand for the ground and the excited states, further show that the apparent exchange rate constant k_{ex} ($k_{ex} = k_{GE} + k_{EG}$) between the folded and unfolded conformations decreases at lower pH, and the relative population p_E of the excited state increases (Fig. 5*A*). The unfolding rate constant k_{GE} is estimated to be ~1.5, 2.0, and 4.1 s^{-1}, whereas the folding rate constant k_{EG} is estimated to be ~500, 218, and 66 s^{-1} at pH 3.5, 3.0, and 2.5, respectively (Table 2).

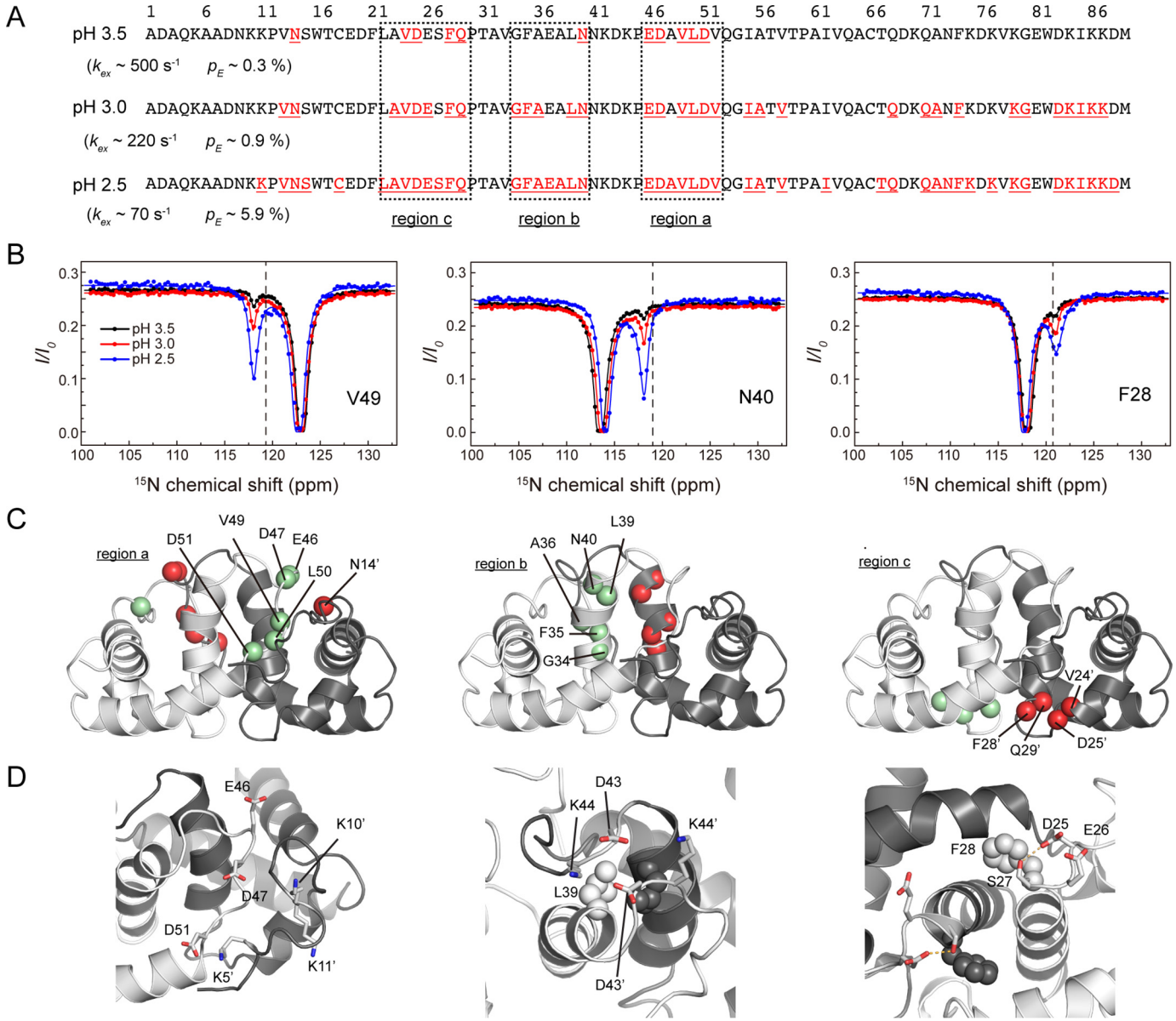

Figure 5. Acid-sensitive structural hot spots identified by CEST NMR. *A,* residues undergoing conformational exchanges identified by the ^{15}N CEST experiments of WT-HdeA at pH 3.5, 3.0, and 2.5 are shown in *red* in the HdeA protein sequence. *Regions a–c* showing sensitive pH responses are depicted by *dashed boxes*. Exchange parameters k_{ex} and p_E estimated from global fitting of the CEST data are shown for each pH condition. *B,* representative ^{15}N CEST profiles of residues in the pH-responsive regions a–c at pH 3.5 (*black*), 3.0 (*red*), and 2.5 (*blue*). The data were obtained using WT-HdeA samples on a 600-MHz spectrometer using a B_1 field of 14.0 Hz and an irradiation period of duration t_{ex} = 800 ms. Intensity ratios I/I_0 were plotted as a function of position of the weak B_1 irradiation field, where I is the intensity after an irradiation period of duration t_{ex} and I_0 is the intensity in the reference experiment where no B_1 field was applied. There is a loss of intensity when the weak continuous-wave field is resonant with the major and minor states. The *dashed lines* indicate the average random coil chemical shift values for the particular amino acid (30). *C,* mapping of the pH-responsive residues in regions a–c onto the HdeA dimer structure. Residues from the two monomers are shown in *green* and *red spheres*, respectively. Residue Asn-14 spatially close to region a is also shown in the *left panel*. *D,* local conformations of regions a–c in the HdeA dimer structure (PDB entry 5WYO in the *left* and *middle panels* and 1DJ8 in the *right panel*) showing the possible electrostatic or hydrogen bond interactions that contribute to structural stabilization. Charged side chains are shown as *sticks*, and hydrophobic side chains are shown a *spheres*. Residues from the second monomer are designated with a ′.

Table 2
Exchange parameters from ^{15}N CEST experiments for WT-HdeA at pH 3.5–2.5

pH	k_{ex}	p_G	k_{GE}	p_E	k_{EG}	τ_E
	s^{-1}	%	s^{-1}	%	s^{-1}	ms
3.5	500 ± 31	99.7 ± 0.1	1.5 ± 0.1	0.3 ± 0.1	498 ± 31	2.0 ± 0.1
3.0	220 ± 5	99.1 ± 0.1	2.0 ± 0.1	0.9 ± 0.1	218 ± 5	4.6 ± 0.1
2.5	70 ± 2	94.1 ± 0.1	4.1 ± 0.1	5.9 ± 0.1	66 ± 2	15.0 ± 0.1

The rate constant of unfolding increases about 3-fold when pH decreases from 3.5 to 2.5, whereas the rate constant of refolding decreases of about 10-fold. These results indicate that the energy barrier for the folding-to-unfolding transition decreases along with the decrease of pH, whereas the energy barrier for the reverse process dramatically increases. This results in a gradual increase of the excited state population, as well as the average lifetime for the excited state, which is ~2.0 ms at pH 3.5, 4.6 ms at pH 3.0, and 15.0 ms at pH 2.5. Moreover, the

estimated unfolding rate constant of 4.1 s^{-1} at pH 2.5 is highly consistent with the kinetics parameter ($k > 3.5\ s^{-1}$) of HdeA unfolding and monomerization reported previously (20), further supporting that the excited states probed by the CEST experiments are on-pathway for HdeA activation.

Conformational transition "hot spots"

By comparing the number and locations of residues showing order-to-disorder exchanges under different pH conditions, we identified three essential acid-sensitive structural hot spots in which conformational transitions (dimer dissociation and unfolding) initially occur (Fig. 5*C*).

The first region (designated as "region a" hereafter) showing quick acid-response at pH 3.5 is the ^{46}ED^{47}–^{49}VLD^{51} segment, which clusters in the C-terminal end of the 50s loop and immediately connects to helix α3. At pH 3.0, one additional residue, Val-52, shows conformational exchanges, whereas at pH 2.5 all residues in the ^{46}EDAVLDV^{52} segment undergo exchanges. Notably, the ^{49}VLDV^{52} tetra-peptide is part of the client-binding site I and is involved in dimer formation by interacting with the N terminus of the other HdeA molecule in the homodimer via electrostatic interactions (Fig. 5*D*). Protonation of the three acidic residues Glu-46, Asp-47, and Asp-51 could break the electrostatic interactions and lead to local structural loosening. Asn-14 residue in the N-terminal loop region is spatially close to the ^{46}ED^{47}–^{49}VLD^{51} segment in the dimer structure (Fig. 5*C*), and its observed conformational exchanges at pH 3.5 could originate from local collective motions.

The second region ("region b") corresponds to segment ^{34}GFA^{36}–^{39}LN^{40} in the C-terminal end of helix α2. Compared with region a, this region shows less acid sensitivity because conformational exchanges could be detected for only Asn-40 at pH 3.5. When the pH decreases to 3.0, conformational exchanges can be observed for residues Gly-34, Phe-35, and Ala-36 located in the very center of the HdeA dimer. The ^{34}GF^{35} dipeptide is part of the client-binding site II, and the Gly-34 and Leu-39 residues have essential contributions to dimer packing by interacting with Gly-34′ and Leu-39′ residues from the other HdeA monomer (here we use a ′ to indicate residues from the second HdeA monomer). Notably, residues Asp-43 and Lys-44 in the loop immediately connected to the C-terminal end of α2 show electrostatic interactions with Asp-43′ and Lys-44′ from the other HdeA monomer (Fig. 5*D*), forming an electrostatic "lock" that helps stabilize the dimeric structure. Protonation of Asp-43 could break this lock and promote the exposure of the client-binding site II.

The third region ("region c") corresponds to the ^{24}VD^{25}–^{28}FQ^{29} segment at the N-terminal tip of helix α2. This region shows relatively high acid sensitivity with four residues exhibiting exchanges at pH 3.5, and the number gradually increases with the decrease in pH values. Notably, the ^{28}FQ^{29} dipeptide is part of the client-binding site II, and the Phe-28 residue contributes to dimer formation by interacting with the Pro-30′ residue. Although the acidic Asp-25 and Glu-26 residues do not show electrostatic contacts with positively charged residues, the carbonyl group of Asp-25 is observed to form a hydrogen bond with the Ser-27 hydroxyl group based on the X-ray crystal structure (Fig. 5*D*). Protonation of the Asp-25 side chain could affect its ability in acting as an electron receptor and destabilize the local structure.

At pH 3.0 and 2.5, residues in other regions also start to show dynamic exchanges between folded and unfolded states, including the hydrophobic ^{55}IA^{56}–V^{58} segment in the α3 helix which may also participate in client interactions, and the densely-charged C-terminal region harboring the α4 helix (Fig. 5*A*).

Multistep activation mechanism of HdeA chaperone function

Based on the above results, a multistep acid–induced activation mechanism of HdeA chaperone function is derived and schematically summarized in Fig. 6. The client-binding site I is located at a relative peripheral region in the HdeA dimer structure and is shielded by the N-terminal segment of the other HdeA molecule. The acidic residues Glu-46, Asp-47, and Asp-51 in the 50s loop have pK_a values of 4.07, 4.14, and 3.83 (22) and are in the deprotonated state under neutral and near-neutral conditions (pH > 4), ensuring electrostatic interaction with the N-terminal region. As the pH decreases to lower than 4, protonation of these residues results in disruption of the intersubunit electrostatic contacts and exposure of the client-binding site I. The self-inhibitory role of the N-terminal region is supported by the observation that an HdeA-NΔ9 mutant with the N-terminal nine residues deleted shows interactions with SurA, another native client of HdeA (13), under elevated pH conditions (Fig. S14, *A* and *B*). In addition, the HdeA-NΔ9 mutant also exhibits partial anti-aggregation activity toward the native client protein OppA (13) at pH 4.0, whereas both WT-HdeA and HdeA-F28W are inactive under this pH condition (Fig. S14*C* and supporting Discussion). Local structural loosening is supported by the sPRE results revealing a drastic difference of the extent of solvent exposure for the N-terminal residues between pH 6 and 4 (Fig. 4), which was not observed in the H/D exchange experiments because all resonances from the N-terminal segment already disappeared even at pH 6 (22). This difference most probably originates from the larger size of the chelated solvent paramagnetic probes compared with water molecules (the probes in the H/D exchange experiments), thus rendering higher sensitivity in observing subtle changes for fast-exchanging amides in the N-terminal segment using the sPRE method.

The client-binding site II located in the α2 helix is tightly packed in the structural core of inactive HdeA dimer and could only be exposed via extensive disruption of the dimeric interface. At pH above 4, two acid-sensitive regions (*region b* and *region c* as shown in Fig. 5) present at both ends of the α2 helix stabilize the dimer interface via inter- and intrasubunit contacts. In addition, previous studies have shown that the protonation of Glu-37, an acidic residue showing an exceptionally high pK_a value, maximally stabilizes the inactive HdeA dimer at pH 5 and protects residues in the client-binding site II from being accessed (10, 22, 31, 32). At pH < 4, acid-induced order-to-disorder conformational exchanges in the b and c acid-sensitive regions loosen the structural locks and enable partial dissociation of the α2 helices of the two HdeA molecules. Notably, region b occupies more than half of the total length of the α2 helix, whereas region c locates only at the N-terminal tip of the helix. Therefore, upon acid-induced loosening of these two

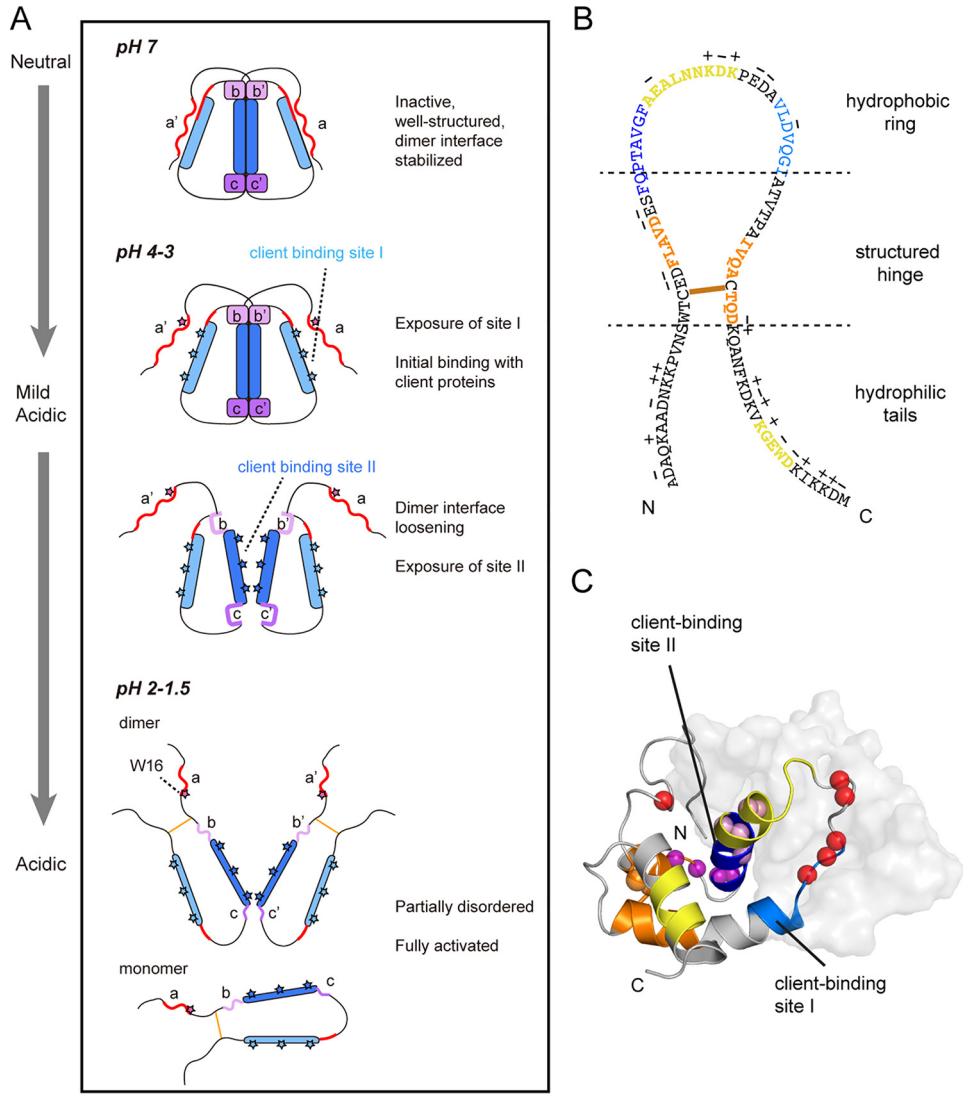

Figure 6. Summary of acid-induced activation mechanism of HdeA. *A,* schematic illustration of the multistep pH-dependent activation process of HdeA. The two client-binding sites I and II are shown in *light blue* and *deep blue*, respectively. As pH decreases, the hydrophobic residues in client-binding sites I and II, as well as the Trp-16 residue, gradually become exposed and competent for client binding (illustrated by *stars*). The pH-sensitive region *a* and the N-terminal segment that regulate the exposure of site I are colored *red*, whereas the pH-sensitive regions *b* and *c* that regulate the exposure of site II are colored *violet* and *purple*, respectively. *B,* illustration of the "ring-tail" model of activated HdeA showing the highly charged hydrophilic tails, the relatively structured hinge containing the disulfide bond, and the hydrophobic ring harboring the client-binding sites I and II. The two sites are colored in *light blue* and *deep blue* as in *A*, and the segments with residual helical contents are colored in *light yellow* (segments 35–43 and 79–83) and *orange* (segments 20–24 and 61–67), respectively. *C,* mapping of all structural features essential to HdeA activation onto the dimer structure. One monomer is shown as a *ribbon* diagram, and the other is shown as the *surface* representation. The client-binding sites and the residual helical regions are colored as in *B*, and the pH-sensitive residues in regions *a*, *b*, and *c* are shown as *spheres* and colored as in *A*.

regions, it appears that the C-terminal part of the α2 helix (the upper part as shown in Figs. 5*C* and 6*A*) becomes more destabilized. The sPRE data at pH 3–4 show that the solvent accessibility of residues in α2 increases rapidly toward the C-terminal end (Fig. 4), further suggesting that the C-terminal half is more significantly affected by pH changes and that dimer dissociation is most probably initiated from this end. This scenario is also supported by previously reported H/D exchange data and molecular dynamics simulations (22, 33).

Taken together, the acid-induced activation of HdeA is a multistep process, which involves the destabilization of three essential structural locks that inhibit the chaperone activity under nonstress conditions. The initial activation step is the dissociation of the N-terminal loop, which exposes the client-binding site I. The subsequent step involves local structural destabilization of helix α2 from both the N- and C-ends, which enables partial exposure of client-binding site II. Finally, when pH further decreases, the whole-protein structure collapses and becomes fully activated, with both sites exposed for client interactions. In the fully activated state, the N- and C-terminal regions of HdeA form two highly charged, flexible "tails" that help increase the solubility of the HdeA–client complexes, whereas the two essentially hydrophobic client-binding sites are held into a "ring" structure by the strictly conserved disulfide bond (Fig. 6, *B* and *C*). Both the spatial proximity of the two client-binding sites restricted by the disulfide bond, as well as the higher propensities of adopting random coil conformations for these two segments compared with other regions in the ring,

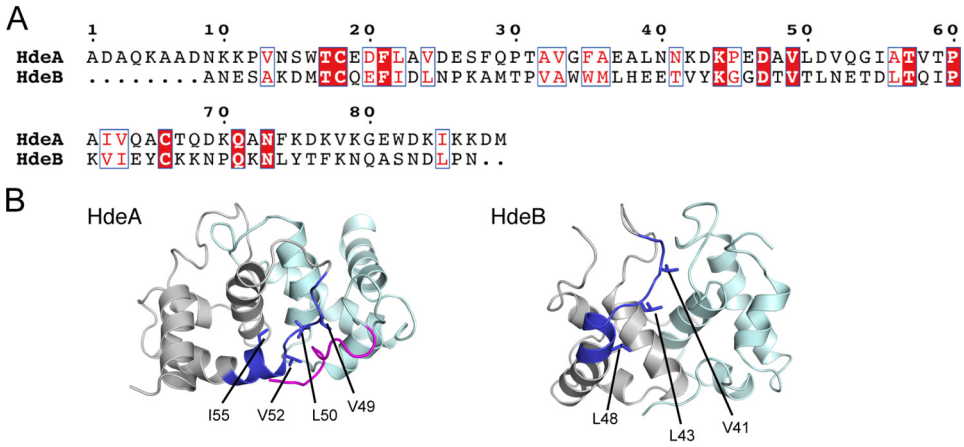

Figure 7. Sequence and structural comparison between HdeA and HdeB. *A,* protein sequence alignment of *E. coli* HdeA and HdeB. *B,* solution structures of dimeric HdeA and HdeB (PDB entries 5WYO and 2MYJ) are shown with the two subunits colored in *gray* and *cyan*, respectively. The segment 47–57 harboring the client-binding site I in HdeA and the corresponding segment in HdeB are colored *blue* in one subunit, and the hydrophobic side chains are shown as *sticks*. The N-terminal nine residues from the other subunit are colored *magenta* in the HdeA dimer structure.

could sufficiently increase the effective hydrophobic surface area to facilitate client interactions.

Self-inhibitory role of the N terminus

In our previous work, we have hypothesized that the N-terminal charged region plays dual roles in HdeA function: one is to increase the HdeA–client complex solubility, and the other is to inhibit the chaperone function under neutral conditions (23). In this study, we show direct evidence that the N terminus protects one of the two essential client-binding sites under non-stress conditions. A previously reported constitutively active HdeA-D20A/D51A double mutant is also consistent with this scenario (10). Based on the solution NMR structure of the inactive HdeA dimer (23), both Asp-51 and Asp-20 play essential roles in stabilizing the N terminus. Asp-51 forms intermolecular contact with Lys-5′, whereas Asp-20 forms intramolecular contact with Lys-11. These two electrostatic interactions, together with the intermolecular electrostatic contacts between Asp-47 and Lys-10′ described above, act in concert to anchor the N terminus onto the surface of the client-binding site I (Fig. S15). Disruption of these interactions could result in the release of the N-terminal region and expose site I under nonacidic conditions. However, we examined the ^{15}N HSQC spectra of the HdeA-D20A/D51A mutant and observed high content of unfolded conformations at pH 7.0 and 5.0 (Fig. S16), which complicates the interpretation of the constitutive chaperone activity at pH $>$ 5 (10). The HdeA-NΔ9 mutant used in this study much better preserves the overall folded structure over the pH range of 7.0 to 3.5 (Fig. S16), and therefore, it provides more direct evidence for the self-regulatory role of the N-terminal segment. Moreover, our model of HdeA activation suggests that the first step of activation occurs at the client-binding site I and involves a simple conformational switch of releasing the N-terminal segment. Thus, without the need for either dimer dissociation or large-scale protein unfolding, HdeA can use this patch of hydrophobic residues for initial contact with partially denatured clients under mild acidic conditions (pH 3.5–3). Actually, this can be supported by the appearance of a few N-terminal signals of HdeA (Lys-5, Ala-6, and Ala-7) when it initially interacts with client proteins at pH 3.0–3.8, as reported in our previous study (23), which highlights the release of the N-terminal segment. No new signals from other regions of HdeA were observed upon client interaction, suggesting that the initial contact involves only site I. More intriguingly, protein sequence alignment of the HdeA and HdeB homologs reveals a nine-residue difference in their N-terminal regions (Fig. 7*A*). The HdeB protein is another acid-resistance chaperone but with a less well understood functional mechanism. The dimeric structures of HdeA and HdeB are significantly different in terms of dimeric packing, although their monomeric structures are essentially similar (34–37). Recent studies both *in vitro* and *in vivo* suggested that HdeB displays optimal chaperone activity at mild acidic pH values (pH ~4) (17, 36). To date, it remains enigmatic as to why HdeB functions at a higher pH range when its overall 3D structure remains intact, whereas HdeA is activated only when it is partially unfolded at lower pH values. Sequence comparison between the two homologs reveals that the most conserved residues between these two proteins are clustered in three regions: the 17–24 and 60–74 segments harboring the consensus cysteines and the 44–58 segment harboring the client-binding site I of HdeA (numbered according to HdeA sequence). The sequence conservation in the first two regions may be important for maintaining structural stability, whereas the conservation in the third region implies that HdeB may also utilize the same site for interaction with client proteins. Because of the lack of the N-terminal nine residues in the HdeB sequence, this site is already exposed and competent for client interactions under nonacidic conditions without the need of protein unfolding (Fig. 7*B*).

Discussion

As Foit *et al.* (10) suggested previously, the activation of HdeA chaperone function may not require the protein to be completely unfolded and that "some of the pH-induced structural changes that accompany HdeA activation are by-products of acidification rather than an actual requirement for activity." Based on residue hydropathy analysis, the hydrophobic segments in the HdeA primary sequence contain 19–41 and 45–65 and span through helices α1, α2, and α3 (19). Our results

show that the client-binding sites (28–35 and 49–55) comprise about only half the length of these segments, whereas hydrophobic residues close to the consensus cysteines are not directly responsible for client interactions. The identified binding sites are consistent with previous findings that hydrophobic residues Phe-35, Val-55, and Val-58 are essential for client interactions (19, 20). Moreover, the two client-binding sites have distinct locations in the HdeA dimer structure and show different pH responses, indicating that HdeA activation follows a pH-dependent stepwise process in which the two sites are activated sequentially and that dimer dissociation (exposure of site II) is more stringently controlled and occurs only at a later stage. Therefore, it is possible that the two sites could act either independently (*e.g.* at mild acidic conditions when the dimer interface remains intact) or in concert with each other to gain higher chaperone activity (at low pH when HdeA is largely unfolded and the two sites are held in close proximity to provide a larger interaction surface). The sequential activation of HdeA may be important for fine-tuning the HdeA–client interactions under different pH conditions.

Although the existence of low-populated partially unfolded intermediates has been suggested by studies from different groups (22, 23, 32, 33, 38, 39), the exact identities of these intermediates and their correlations with chaperone function were poorly understood. Several molecular simulation studies have been carried out (31, 33, 38–40), and a partially unfolded dimeric intermediate (I_2) of HdeA was captured showing the characteristics of an almost intact dimeric interface, whereas the helix α4 in one monomer is largely disordered (33). However, the location of the two client-binding sites indicates that unfolding and dissociation of helix α4 from the structural core does not play a profound role in exposing the hydrophobic surface responsible for client binding. Inspection of the HdeA dimer structure reveals that the side chains of Phe-74, Val-78, and Trp-82 from helix α4 form a hydrophobic core within a monomer with Phe-21 from helix α1, Val-33 from helix α2, and Val-58 and Ile-62 from helix α3, but are distal from either the Val-49/Ile-55 residues in client-binding site I or the bulky aromatic side chains of Phe-28/Phe-35 in client-binding site II (Fig. S17). Therefore, unfolding of helix α4 within a monomer would not lead to significant exposure of the two hydrophobic binding sites. More importantly, the CEST data indicates that local structure loosening at the three pH-sensitive hot spots starts at a higher pH (pH 3.5) than the unfolding of helix α4 (pH 3.0). Unlike the drastic conformational change associated with helix α4 unfolding, these earlier structural loosening events at the pH-sensitive regions occur in a much more localized manner, but are directly involved in the exposure of client-binding sites and thus are more correlated with the chaperone activity. Taken together, the unfolding of α4 is more likely to be a by-product of HdeA structural changes induced by acidification. Nevertheless, unfolding of α4 may contribute to increasing HdeA chaperone activity at low pH by exposing the 58–63 segment in helix α3 as an extension to the client-binding site I. Additionally, it is also possible that α4 unfolding could indirectly affect the stability of the dimeric interface and facilitate dimer dissociation. It is worth mentioning that all computational studies aimed at characterizing the unfolding intermediates of HdeA reported thus far start from the crystal structure lacking the first nine residues (10, 31, 33, 38–40), and any local conformational changes involving the N-terminal segment would have gone unnoticed. Our current CEST data may hopefully provide an experimental basis and aid further molecular simulation studies.

Although the structural details of chaperone–client complexes are usually difficult to investigate due to the large molecular sizes and conformational dynamics, recent advances in solution NMR methods have enabled atomic-resolution structural determinations of the chaperones trigger factor (TF) and SecB in complex with unfolded clients (41, 42). The bacterial acid-response chaperone HdeA exhibits some unique characteristics compared with these chaperone systems as it is largely disordered and dynamic in the activated state, whereas TF and SecB adopt relatively rigid three-dimensional structures with hydrophobic client-binding sites spread out on their surfaces. The two client-binding sites in HdeA are hydrophobic, which is a common feature shared among different chaperones. However, the extremely small molecular size of HdeA and the fact that the two client binding segments become largely disordered upon activation suggest that the HdeA–client binding mode could be much different from the above two chaperones. The disordered characteristics of the binding sites in HdeA may provide better exposure of the hydrophobic side chains and are favorable for client interactions. The observation that the binding sites show more extended conformations compared with neighboring regions suggests an inverse correlation between the helical-forming propensity and the client-binding activity and provides a unique demonstration of the link between structure disorder and chaperone function. Alternatively, the client-binding sites may adopt transiently formed or sparsely populated helical structures (in particular, residues in site I are estimated to have 10–20% of helix-forming propensities), which may fine-tune the local conformation and facilitate promiscuous binding to a broad range of client proteins. Moreover, considering the results that segments outside the two client-binding sites show relatively high helix-forming propensities under acidic conditions and that the HdeA-V33K and L50K mutations simultaneously destabilize inactive dimer structure and impair the chaperone activity, it is possible that a partially folded conformation of HdeA may be needed for sufficient chaperone–client complex formation. This scenario is also consistent with the observations that the disulfide bridge was important for chaperone function (20) and that the conformational transition hot spots identified by CEST cluster in space in the inactive state of HdeA. Under extremely acidic conditions when HdeA becomes largely unfolded, it remains possible that the chaperone transiently excurses to a partially folded state that facilitates complex formation with clients.

Taken together, our data highlight a complex interplay of both protein structural order and disorder in the regulation of the HdeA chaperone function. To fully understand the functional mechanism of HdeA, the atomic-level structural information concerning HdeA–client complexes is essential. The mode of HdeA–client interactions could be different under

mild acidic and highly acidic conditions, which have potential physiological implications regarding responses to different extents of acid stress, cooperation between HdeA and HdeB homologs, as well as the process of client release (21). However, the disappearance of NMR signals in the ^{1}H-^{15}N HSQC spectra of HdeA upon complex formation most probably reflects the promiscuous and dynamic nature of the binding, and it renders atomic-resolution structural determination of HdeA–client complexes through similar approaches as used in the studies of TF and SecB exceptionally difficult. Moreover, much less is known about the conformational states of acid-denatured client proteins and their chaperone-interacting sites, and further investigations focusing on the clients would hopefully shed more light on the HdeA–client interactions.

Experimental procedures

Sample preparations

The *Escherichia coli hdeA, malE, surA,* and *oppA* genes and all *hdeA* mutant genes were cloned into pET-28a(+) plasmid (Novagen) and transformed into *E. coli* BL21(DE3)-T1R or BL21 Star(DE3)-T1R strains (Sigma) for protein expression. All protein expression and purification procedures were similar, as reported previously (23). The NMR samples were prepared in buffers containing 50 mM sodium phosphate and 45 mM citric acid at different pH conditions. The HdeA–client complex samples were prepared by mixing the HdeA and client protein samples at pH 7 and subsequently changing into buffers with various pH values using Millipore centrifugation tubes with a 3-kDa molecular mass cutoff.

Anti-aggregation assay

The chaperone activities of WT-HdeA, the HdeA-F28W mutant, and all ^{19}F-labeling mutants were tested by the anti-aggregation assay as reported previously (9, 43). MalE was used as the client protein and incubated in a buffer containing 45 mM citric acid, 50 mM sodium phosphate, and 150 mM sodium sulfate (pH 1.5) at 25 °C for 60 min with or without the presence of HdeA and its mutants. The addition of 150 mM sodium sulfate was to achieve effective aggregation of MalE at low pH values (44, 45). The MalE concentration was kept at 10 μM, whereas four different concentrations (1, 2.5, 5, and 10 μM) were used for HdeA and its mutants. The presence of MalE in the supernatant or the pellet was analyzed by SDS-PAGE.

For measuring the anti-aggregation activity of the HdeA-NΔ9 mutant at pH 4.0, the client protein OppA was used, and the incubation temperature was increased to 35 °C. All other experimental conditions were the same. Control experiments were performed using WT-HdeA and HdeA-F28W at both pH 4.0 and 1.5.

Chemical shift assignments of the F28W mutant at low pH

For chemical shift assignments of the active monomeric state of HdeA, a sample containing 0.5 mM $^{13}C/^{15}N$-labeled HdeA-F28W mutant was prepared at pH 1.5. NMR spectra were acquired at 25 °C on Bruker Avance 700-MHz spectrometers, equipped with four RF channels and a triple-resonance cryoprobe with pulsed field gradients. Two-dimensional ^{15}N-edited HSQC spectroscopy, traditional three-dimensional HNCA, HN(CO)CA, HNCACB, HN(CO)CACB, HNCO, and HN(CA)CO for protein backbone assignments, as well as HNN and HN(C)N experiments especially designed for assigning unfolded proteins were collected (46, 47). All spectra were processed using the software package NMRPipe (48) and analyzed by the program NMRView (49).

^{19}F labeling

Site-specific incorporation of ^{19}F labels into HdeA was achieved by labeling tryptophan residues with 5-fluorotryptophan following published methods (50). Briefly, *E. coli* cells harboring plasmids containing the mutant genes were first grown in 1 liter of Luria-Bertani medium at 35 °C. When the A_{600} reached 0.8, the cells were collected by centrifugation at 4000 × *g* and resuspended in 500 ml of M9 minimal medium with NH_4Cl and glucose as the nitrogen and carbon sources, 60 mg/liter 5-fluoroindole, and with 50 mg/liter kanamycin. After shaking for 1 h at 35 °C, protein expression was induced by adding isopropyl β-D-thiogalactoside to a final concentration of 0.4 mM. Cells were grown for another 8 h and harvested by centrifugation. $^{15}NH_4Cl$ was used in the M9 media to simultaneously achieve site-specific ^{19}F incorporation and uniform ^{15}N labeling. The WT-HdeA protein sequence contains two tryptophan residues Trp-16 and Trp-82. For ^{19}F labeling in these two sites, the HdeA W82F or W16F mutants were used. For ^{19}F labeling in all other sites, additional mutations were made based on the HdeA W16F/W82F double mutant (*e.g.* for ^{19}F labeling in position 39, a HdeA W16F/W82F/L39W triple mutant was used).

^{19}F NMR experiments

^{19}F NMR experiments were performed at pH 7.0 or 2.0. The preparations for the samples containing $^{15}N/^{19}F$-labeled HdeA mutants alone or in complex with unlabeled substrate MalE at pH 2.0 were similar to those reported previously (23). The samples were prepared with 0.5 mM $^{15}N/^{19}F$-labeled HdeA mutants with or without 1.0 mM MalE for the free or complexed states, respectively. Trifluoroacetic acid (TFA) was added to a final concentration of 10 μM as the internal chemical shift reference. All samples were prepared using the same stock of buffers with different pH values, and the exact pH value for each sample was further measured using microelectrode as well as ^{19}F NMR of a chemical shift-based pH sensor 4-fluoroaniline, as described previously (23). One-dimensional ^{19}F NMR spectra were acquired on a Bruker 600-MHz spectrometer equipped with a room temperature BBO probe at 25 °C. For all ^{19}F-labeled mutants, the spectra of the inactive free state (pH 7), the active free state (pH 2), and the complex state (pH 2) were acquired sequentially, and a standard methanol sample was used for temperature calibration to ensure that the temperature control system of the spectrometer remained stable over time. A spectral width of 12 kHz and a relaxation delay of 1.5 s were used. A total of 4096 or 100,000 transients was recorded for the free state or HdeA–MalE complex samples, respectively.

For measuring the solvent-induced isotope shifts, the samples were initially prepared in a buffer containing 90% H_2O and 10% D_2O for NMR spectra collection and subsequently lyoph-

ilized and re-dissolved in 100% D_2O for another round of ^{19}F NMR spectra measurement. The solvent-induced isotope shift $\Delta\delta$ values reported in this study are calculated as $\Delta\delta = \delta(D_2O) - \delta(H_2O)$, where $\delta(D_2O)$ is the ^{19}F chemical shift measured in 100% D_2O, and $\delta(H_2O)$ is the ^{19}F chemical shift measured in 90% H_2O and 10% D_2O. The concentration of D_2O in all samples was carefully controlled. The sample preparations and NMR measurements were repeated to confirm that the ^{19}F NMR spectra were well-reproduced and to estimate the data uncertainties. The solvent-induced isotope shifts $\Delta\delta$ were also measured at pH 7.0 as a control, where we observed that residues in flexible regions show $|\Delta\delta|$ values in the range of 0.10 to 0.17 ppm, whereas the $|\Delta\delta|$ value for TFA in 100% D_2O and in 90% H_2O, 10% D_2O was 0.14 ppm.

Apart from the solvent isotope shifts, the ^{19}F spectra of the HdeA mutants in complex with MalE acquired before and after lyophilization are essentially identical in terms of shape and line widths, indicating that lyophilization does not change the structure of HdeA in the complex or the mode of interaction between HdeA and the client. This was further verified by the essential similarity between the ^1H NMR spectra of the HdeA–MalE complexes at pH 2.0 before and after lyophilization (the samples were re-dissolved in H_2O so that that no hydrogen–deuterium exchange occurs).

ITC experiments

Binding of HdeA or its mutants to the client MalE was measured by ITC using a VP-ITC microcalorimeter (MicroCal, Northampton, MA) at 25 °C according to the manufacturer's instructions. All protein samples were dialyzed overnight against a buffer containing 45 mM citric acid and 50 mM sodium phosphate (pH 1.5) and were degassed for 10 min before the titrations. A total of 283 μl of concentrated WT-HdeA or its mutants (235 μM) was used as the titrant and added into the MalE solution (1400-μl, 19 μM). The titrations were carried out with a preliminary 2-μl injection (discarded in the data analyses) and followed by 24 injections of 10 μl with an interval of 300 s. The control experiment by titrating HdeA into the buffer was subtracted before data analyses. Note that the buffer used for the ITC measurements does not contain the 150 mM sodium sulfate, which is different from the buffer used in the anti-aggregation assay, so that the MalE protein remains soluble under the experimental condition. All data were analyzed using the program package PEAQ-ITC analysis (Microcal) with different binding models, and the standard errors of the extracted parameters were derived from nonlinear least-squares fitting using the Levenberg-Marquardt algorithm.

sPRE experiments

Paramagnetic samples were prepared with ^{15}N-labeled HdeA (0.6 mM) with paramagnetic probe EDTA-Gd^{3+} (0.5 mM), whereas the diamagnetic samples were prepared with ^{15}N-labeled HdeA alone. An excess of EDTA (1.0 mM) is added in both samples to eliminate the binding of Gd^{3+} ions onto the protein. The ^1H-^{15}N HSQC spectra were collected for both samples at pH conditions of 6.0, 4.0, and 3.0 on a Bruker Avance 800-MHz spectrometer at 25 °C. The spectra of the paramagnetic and diamagnetic samples at each pH condition were carefully compared to ensure that the addition of the EDTA-Gd^{3+} probe did not affect the sample pH and that all signals were well overlaid. The sPRE effects were calculated as the intensity ratio for each residue in the spectra of the paramagnetic and diamagnetic samples. The experimental errors were determined from duplicated experiments.

^{15}N CEST measurements and analysis

The ^{15}N CEST experiment (29) for WT-HdeA was acquired at 35 °C on a Bruker Avance 600-MHz spectrometer. Comparisons of the HSQC spectra and CEST profiles at three different temperatures, 15, 25, and 35 °C, demonstrate that the structure and conformational exchanges are essentially similar, but acquiring CEST data at 35 °C provided the highest sensitivity. The sample was prepared in buffers containing 50 mM phosphate, 45 mM citric acid, and 10% D_2O at pH 4.0, 3.5, 3.0, and 2.5 with the protein concentrations of 2.0 mM. A total of 105 2D data sets were acquired with the ^{15}N carrier frequencies positioned from 101 to 132.2 ppm at a spacing of 0.3 ppm (18.24 Hz) during the irradiation time of t_{ex} = 800 ms. In all experiments, irradiation field strengths B_1 of 9.4 ± 0.2 and 14.0 ± 0.2 Hz were used, and a 2.7-kHz field ^1H decoupling composite pulse sequence (90_x–240_y–90_x) was applied during the t_{ex} period. Data without using the B_1 field during the t_{ex} period was recorded as the reference experiment. B_1 calibration was carried out following the previously reported methods (51). All the data sets were processed using the NMRPipe program (48), and peak intensities were obtained by NMRView (49). The CEST profiles for the individual residues were generated by calculating the intensity ratios I/I_0 *versus* the varied ^{15}N carrier frequencies, where I_0 is the intensity measured in the reference spectrum, and I is the intensity measured with the application of the B_1 field. The CEST data were analyzed using the software package ChemEx (https://github.com/gbouvignies/chemex)[6] or in-house written Matlab scripts from B. Yu and D. Yang (52).

For a two-state exchange process, $G \underset{k_{EG}}{\overset{k_{GE}}{\rightleftharpoons}} E$, G and E represent the ground state and sparsely populated excited state, respectively. The fractional populations of two states p_G and p_E satisfy the equations $p_G = k_{EG}/k_{ex}$ and $p_E = k_{GE}/k_{ex}$, with $k_{ex} = k_{GE} + k_{EG}$, $p_G + p_E = 1$, and $p_G \gg p_E$. The lifetime of the excited state E is given by $\tau_E = 1/k_{EG}$, and the rate constants k_{GE} and k_{EG} can be calculated as $k_{GE} = k_{ex} \cdot p_E$ and $k_{EG} = k_{ex} \cdot p_G$. The uncertainties of peak intensities were estimated from repeat measurements, and the standard errors of the extracted kinetic parameters were determined from data fitting by the ChemEx software using the covariance matrix.

Author contributions—X.-C. Y. and J. D. investigation; X.-C. Y. visualization; X.-C. Y. and Y. H. writing-original draft; Y. H. and C. J. funding acquisition; Y. H. validation; Y. H. project administration; Y. H. and C. J. writing-review and editing; H. L. methodology; C. J. conceptualization; C. J. supervision.

[6] Please note that the JBC is not responsible for the long-term archiving and maintenance of this site or any other third party hosted site.

Acknowledgments—All NMR experiments were performed at the Beijing NMR Center and the NMR facility of National Center for Protein Sciences at Peking University. We thank Prof. Zongchao Jia from Queen's University, Canada, for critical reading of the manuscript and helpful suggestions. We thank Prof. Zhixin Wang and Prof. Jiawei Wu from Tsinghua University, China, for the kind support in the ITC measurements.

References

1. Toth-Petroczy, A., Palmedo, P., Ingraham, J., Hopf, T. A., Berger, B., Sander, C., and Marks, D. S. (2016) Structured states of disordered proteins from genomic sequences. *Cell* **167,** 158–170.e12 CrossRef Medline
2. Tompa, P. (2012) Intrinsically disordered proteins: a 10-year recap. *Trends Biochem. Sci.* **37,** 509–516 CrossRef Medline
3. Marín, M., Uversky, V. N., and Ott, T. (2013) Intrinsic disorder in pathogen effectors: protein flexibility as an evolutionary hallmark in a molecular arms race. *Plant Cell* **25,** 3153–3157 CrossRef Medline
4. Gu, S., Shevchik, V. E., Shaw, R., Pickersgill, R. W., and Garnett, J. A. (2017) The role of intrinsic disorder and dynamics in the assembly and function of the type II secretion system. *Biochim. Biophys. Acta* **1865,** 1255–1266 CrossRef
5. Bardwell, J. C., and Jakob, U. (2012) Conditional disorder in chaperone action. *Trends Biochem. Sci.* **37,** 517–525 CrossRef Medline
6. Reichmann, D., Xu, Y., Cremers, C. M., Ilbert, M., Mittelman, R., Fitzgerald, M. C., and Jakob, U. (2012) Order out of disorder: working cycle of an intrinsically unfolded chaperone. *Cell* **148,** 947–957 CrossRef Medline
7. Franzmann, T. M., Menhorn, P., Walter, S., and Buchner, J. (2008) Activation of the chaperone Hsp26 is controlled by the rearrangement of its thermosensor domain. *Mol. Cell* **29,** 207–216 CrossRef Medline
8. Jaya, N., Garcia, V., and Vierling, E. (2009) Substrate binding site flexibility of the small heat shock protein molecular chaperones. *Proc. Natl. Acad. Sci. U.S.A.* **106,** 15604–15609 CrossRef Medline
9. Hong, W., Jiao, W., Hu, J., Zhang, J., Liu, C., Fu, X., Shen, D., Xia, B., and Chang, Z. (2005) Periplasmic protein HdeA exhibits chaperone-like activity exclusively within stomach pH range by transforming into disordered conformation. *J. Biol. Chem.* **280,** 27029–27034 CrossRef Medline
10. Foit, L., George, J. S., Zhang, B. W., Brooks, C. L., 3rd., and Bardwell, J. C. (2013) Chaperone activation by unfolding. *Proc. Natl. Acad. Sci. U.S.A.* **110,** E1254–E1262 CrossRef Medline
11. Wright, P. E., and Dyson, H. J. (2009) Linking folding and binding. *Curr. Opin. Struct. Biol.* **19,** 31–38 CrossRef Medline
12. Bah, A., and Forman-Kay, J. D. (2016) Modulation of intrinsically disordered protein function by post-translational modifications. *J. Biol. Chem.* **291,** 6696–6705 CrossRef Medline
13. Gajiwala, K. S., and Burley, S. K. (2000) HDEA, a periplasmic protein that supports acid resistance in pathogenic enteric bacteria. *J. Mol. Biol.* **295,** 605–612 CrossRef Medline
14. Hong, W., Wu, Y. E., Fu, X., and Chang, Z. (2012) Chaperone-dependent mechanisms for acid resistance in enteric bacteria. *Trends Microbiol.* **20,** 328–335 CrossRef Medline
15. Hingorani, K. S., and Gierasch, L. M. (2013) How bacteria survive an acid trip. *Proc. Natl. Acad. Sci. U.S.A.* **110,** 5279–5280 CrossRef Medline
16. Zhang, M., Lin, S., Song, X., Liu, J., Fu, Y., Ge, X., Fu, X., Chang, Z., and Chen, P. R. (2011) A genetically incorporated crosslinker reveals chaperone cooperation in acid resistance. *Nat. Chem. Biol.* **7,** 671–677 CrossRef Medline
17. Zhang, S., He, D., Yang, Y., Lin, S., Zhang, M., Dai, S., and Chen, P. R. (2016) Comparative proteomics reveal distinct chaperone–client interactions in supporting bacterial acid resistance. *Proc. Natl. Acad. Sci. U.S.A.* **113,** 10872–10877 CrossRef Medline
18. Yang, F., Gustafson, K. R., Boyd, M. R., and Wlodawer, A. (1998) Crystal structure of *Escherichia coli* HdeA. *Nat. Struct. Biol.* **5,** 763–764 CrossRef Medline
19. Wu, Y. E., Hong, W., Liu, C., Zhang, L., and Chang, Z. (2008) Conserved amphiphilic feature is essential for periplasmic chaperone HdeA to support acid resistance in enteric bacteria. *Biochem. J.* **412,** 389–397 CrossRef Medline
20. Tapley, T. L., Körner, J. L., Barge, M. T., Hupfeld, J., Schauerte, J. A., Gafni, A., Jakob, U., and Bardwell, J. C. (2009) Structural plasticity of an acid-activated chaperone allows promiscuous substrate binding. *Proc. Natl. Acad. Sci. U.S.A.* **106,** 5557–5562 CrossRef Medline
21. Tapley, T. L., Franzmann, T. M., Chakraborty, S., Jakob, U., and Bardwell, J. C. (2010) Protein refolding by pH-triggered chaperone binding and release. *Proc. Natl. Acad. Sci. U.S.A.* **107,** 1071–1076 CrossRef Medline
22. Garrison, M. A., and Crowhurst, K. A. (2014) NMR-monitored titration of acid-stress bacterial chaperone HdeA reveals that Asp and Glu charge neutralization produces a loosened dimer structure in preparation for protein unfolding and chaperone activation. *Protein Sci.* **23,** 167–178 CrossRef Medline
23. Yu, X. C., Yang, C., Ding, J., Niu, X., Hu, Y., and Jin, C. (2017) Characterizations of the interactions between *Escherichia coli* periplasmic chaperone HdeA and its native substrates during acid stress. *Biochemistry* **56,** 5748–5757 CrossRef Medline
24. Burmann, B. M., and Hiller, S. (2015) Chaperones and chaperone-substrate complexes: dynamic playgrounds for NMR spectroscopists. *Prog. Nucl. Magn. Reson. Spectrosc.* **86,** 41–64 Medline
25. Sekhar, A., and Kay, L. E. (2013) NMR paves the way for atomic level descriptions of sparsely populated, transiently formed biomolecular conformers. *Proc. Natl. Acad. Sci. U.S.A.* **110,** 12867–12874 CrossRef Medline
26. Kitevski-LeBlanc, J. L., and Prosser, R. S. (2012) Current applications of ^{19}F NMR to studies of protein structure and dynamics. *Prog. Nucl. Magn. Reson. Spectrosc.* **62,** 1–33 CrossRef Medline
27. Marsh, J. A., Singh, V. K., Jia, Z., and Forman-Kay, J. D. (2006) Sensitivity of secondary structure propensities to sequence differences between α- and γ-synuclein: implications for fibrillation. *Protein Sci.* **15,** 2795–2804 CrossRef Medline
28. Zhai, Z., Wu, Q., Zheng, W., Liu, M., Pielak, G. J., and Li, C. (2016) Roles of structural plasticity in chaperone HdeA activity are revealed by ^{19}F NMR. *Chem. Sci.* **7,** 2222–2228 CrossRef Medline
29. Vallurupalli, P., Bouvignies, G., and Kay, L. E. (2012) Studying "invisible" excited protein states in slow exchange with a major state conformation. *J. Am. Chem. Soc.* **134,** 8148–8161 CrossRef Medline
30. Schwarzinger, S., Kroon, G. J., Foss, T. R., Wright, P. E., and Dyson, H. J. (2000) Random coil chemical shifts in acidic 8 M urea: implementation of random coil shift data in NMRView. *J. Biomol. NMR* **18,** 43–48 CrossRef Medline
31. Zhang, B. W., Brunetti, L., and Brooks, C. L., 3rd (2011) Probing pH-dependent dissociation of HdeA dimers. *J. Am. Chem. Soc.* **133,** 19393–19398 CrossRef Medline
32. Salmon, L., Stull, F., Sayle, S., Cato, C., Akgül Ş., Foit, L., Ahlstrom, L. S., Eisenmesser, E. Z., Al-Hashimi, H. M., Bardwell, J. C. A., and Horowitz, S. (2018) The mechanism of HdeA unfolding and chaperone activation. *J. Mol. Biol.* **430,** 33–40 CrossRef Medline
33. Ahlstrom, L. S., Dickson, A., and Brooks, C. L., 3rd (2013) Binding and folding of the small bacterial chaperone HdeA. *J. Phys. Chem. B* **117,** 13219–13225 CrossRef Medline
34. Kern, R., Malki, A., Abdallah, J., Tagourti, J., and Richarme, G. (2007) *Escherichia coli* HdeB is an acid stress chaperone. *J. Bacteriol.* **189,** 603–610 CrossRef Medline
35. Wang, W., Rasmussen, T., Harding, A. J., Booth, N. A., Booth, I. R., and Naismith, J. H. (2012) Salt bridges regulate both dimer formation and monomeric flexibility in HdeB and may have a role in periplasmic chaperone function. *J. Mol. Biol.* **415,** 538–546 CrossRef Medline
36. Dahl, J. U., Koldewey, P., Salmon, L., Horowitz, S., Bardwell, J. C., and Jakob, U. (2015) HdeB functions as an acid-protective chaperone in bacteria. *J. Biol. Chem.* **290,** 65–75 CrossRef Medline
37. Ding, J., Yang, C., Niu, X., Hu, Y., and Jin, C. (2015) HdeB chaperone activity is coupled to its intrinsic dynamic properties. *Sci. Rep.* **5,** 16856 CrossRef Medline
38. Ahlstrom, L. S., Law, S. M., Dickson, A., and Brooks, C. L., 3rd (2015) Multiscale modeling of a conditionally disordered pH-sensing chaperone. *J. Mol. Biol.* **427,** 1670–1680 CrossRef Medline

39. Dickson, A., Ahlstrom, L. S., and Brooks, C. L., 3rd (2016) Coupled folding and binding with 2D window-exchange umbrella sampling. *J. Comput. Chem.* **37,** 587–594 CrossRef Medline
40. Socher, E., and Sticht, H. (2016) Probing the structure of the *Escherichia coli* periplasmic proteins HdeA and YmgD by molecular dynamics simulations. *J. Phys. Chem. B* **120,** 11845–11855 CrossRef Medline
41. Saio, T., Guan, X., Rossi, P., Economou, A., and Kalodimos, C. G. (2014) Structural basis for protein antiaggregation activity of the trigger factor chaperone. *Science* **344,** 1250494 CrossRef Medline
42. Huang, C., Rossi, P., Saio, T., and Kalodimos, C. G. (2016) Structural basis for the antifolding activity of a molecular chaperone. *Nature* **537,** 202–206 CrossRef Medline
43. Malki, A., Le, H. T., Milles, S., Kern, R., Caldas, T., Abdallah, J., and Richarme, G. (2008) Solubilization of protein aggregates by the acid stress chaperones HdeA and HdeB. *J. Biol. Chem.* **283,** 13679–13687 CrossRef Medline
44. Goto, Y., and Fink, A. L. (1989) Conformational states of β-lactamase: molten-globule states at acidic and alkaline pH with high salt. *Biochemistry* **28,** 945–952 CrossRef Medline
45. Goto, Y., Takahashi, N., and Fink, A. L. (1990) Mechanism of acid-induced folding of proteins. *Biochemistry* **29,** 3480–3488 CrossRef Medline
46. Sattler, M., Schleucher, J., and Griesinger, C. (1999) Heteronuclear multidimensional NMR experiments for the structure determination of proteins in solution employing pulsed field gradients. *Prog. Nucl. Magn. Reson. Spectrosc.* **34,** 93–158 CrossRef
47. Panchal, S. C., Bhavesh, N. S., and Hosur, R. V. (2001) Improved 3D triple resonance experiments, HNN and HN(C)N, for HN and ^{15}N sequential correlations in (^{13}C, ^{15}N) labeled proteins: application to unfolded proteins. *J Biomol. NMR* **20,** 135–147 CrossRef Medline
48. Delaglio, F., Grzesiek, S., Vuister, G. W., Zhu, G., Pfeifer, J., and Bax, A. (1995) NMRPipe: a multidimensional spectral processing system based on UNIX pipes. *J Biomol. NMR* **6,** 277–293 Medline
49. Johnson, B. A. (2004) Using NMRView to visualize and analyze the NMR spectra of macromolecules. *Methods Mol. Biol.* **278,** 313–352 Medline
50. Crowley, P. B., Kyne, C., and Monteith, W. B. (2012) Simple and inexpensive incorporation of ^{19}F-tryptophan for protein NMR spectroscopy. *Chem. Commun.* **48,** 10681–10683 CrossRef
51. Yuwen, T., and Kay, L. E. (2017) Longitudinal relaxation optimized amide ^{1}H-CEST experiments for studying slow chemical exchange processes in fully protonated proteins. *J. Biomol. NMR* **67,** 295–307 CrossRef Medline
52. Yu, B., and Yang, D. (2016) Coexistence of multiple minor states of fatty acid binding protein and their functional relevance. *Sci. Rep.* **6,** 34171 CrossRef Medline